Electronic Supplementary Information

Promoting Structural Distortion to Enhance Crystal Field Strength of Mn (II) in Tetrahedral Bromide for Near-Unity Yellow Emission

Zhikai Qi,‡*[a] Ke Zhang,‡[a] Xingxing Zhao,[a] Nan Zhang,[a] Shi-Li Li[a] and Xian-Ming Zhang*[ab]

[a] *Key Laboratory of Magnetic Molecules & Magnetic Information Materials (Ministry of Education), School of Chemistry and Material Science, Shanxi Normal University, Taiyuan 030006, P. R. China. E-mail: qizk@sxnu.edu.cn, zhangxm@sxnu.edu.cn.*
[b] *College of Chemistry, Taiyuan University of Technology, Taiyuan 030024, P. R. China.*
‡ *These authors contributed equally to this work.*

Contents

1.Experimental section

1.1 Reagents and Syntheses. All chemicals were analytically pure and commercially available, which were directly used without any further purification. $MnBr_4 \cdot 4H_2O$ (0.224 g, 0.1mmol) with 4-2-aminomethylpyridine (0.122 g, 0.1mmol) was first dissolved in ethanol (4 mL) and later acidified by adding bromic acid (1 mL). The mixture was stirred for 30 min under 60 °C until the solid powder was completely dissolved to give a clear aqueous solution. Upon gradual evaporation of the solvent over a period of 48 hours, light-yellow crystals of **1** emerged. As the solvent volume diminished over time, we observed that after 72 h the resultant crystals (**2**) emits a distinct bright yellow light. We collected the PXRD data and PL spectra of **1**, **2**, and the sample with mixed phases at some point and found that both the peak position and bandwidth fall in between **1** and **2** (Fig. S11), indicating that the sample contains two kinds of crystal phases and the phase transformation is going on. Moreover, FT-IR spectra in Fig. S12 show characteristic peaks at 1572 and 1652 cm^{-1} corresponding to the pyridine ring, indicating that the organic template cations are integrate into the hybrids. Thermogravimetric analysis (TGA) demonstrates that two halides have high thermal stability up to 571K (Fig. S13).

1.2 X-ray Crystallographic Study. Single-crystal X-ray diffraction data of **1** and **2** were collected using an Agilent single crystal diffractometer with Mo Kα radiation (λ=0.71073Å). The crystal structure of **1** and **2** was solved directly using the SHELXL-97 package on the Olex2 software. This was followed by full matrix least-squares minimi sation of F^2 with anisotropic refinement of Mn, Br, C and N atoms. In theory, all of the H atoms in the organic cations are generated on top of C and N atoms using isotropic refinement. Table S2 and Table S3 give crystallographic data for some of the bond lengths and angles in the structures.

1.3 Photoluminescence measurements. The photoluminescence (PL) measurements of **1** and **2**, involving excitation spectrum, temperature-dependent PL spectra, and time-resolved decay data, were performed on an Edinburgh FLS-920 fluorescence spectrometer with a picosecond pulsed diode laser. PLQY was also achieved using

FLS-920 spectrofluorometer equipped with an integrating sphere. The equation: $\eta_{QE} = I_S/(E_R - E_S)$ was used to calculate PLQY, where I_S stands for the emission spectra of the compound, E_R is the spectra of the excitation light of the empty integrated sphere, and E_S is the excitation spectra of the excited sample. The CIE chromaticity coordinates were calculated using the CIE calculator software based on the emission spectra. The emission spectra, correlated color temperature (CCT), luminous efficacy, and CIE coordinates of white LED device were performed on the integrating sphere spectroradiometer system (ATA-100, Everfine, EOS, Hangzhou, China).

1.4 Characterization. TU-1950 UV spectrometer was used to record the UV-vis absorption curves of two halides at ambient condition, where the standard reference was $BaSO_4$. Powder X-ray diffraction (XRD) measurements were measured at 40 kV and 100 mA on a Rigaku D/Max-2500 diffractometer with Cu Kα radiation, and the powder diffraction patterns were collected in the 2θ range of 5° to 50° with a step size of 0.02 min^{-1}.TGA measurement was carried out on a NETZSCH STA 449F3 thermal analyzer under N_2 at a heating rate of 10 °C/min.

1.5 Hirshfeld surface analysis. Hirshfeld surfaces and related two-dimensional (2D) fingerprints of $DMAPH^+$ cations in the asymmetric unit of **1** and **2** were calculated using Crystal Explorer 21.5 program with inputting structure file in CIF format. In this work, all the Hirshfeld surfaces were generated using a standard (high) surface resolution. The three-dimensional (3D) Hirshfeld surfaces and 2D fingerprint plots are unique for any crystal structure. The intensity of intermolecular interaction is mapped onto the Hirshfeld surface by using the respective red-blue-white scheme: where the white or green regions exactly correspond to the distance of van der Waals contact, the blue regions correspond to longer contacts, and the red regions represent closer contacts. In 2D fingerprint plots, each point represents an individual pair (d_i, d_e), reflecting the distances to the nearest atom inside (d_i) and outside (d_e) of the Hirshfeld surface, and the frequency of occurrence for these points correspond to the color from blue (low), through green, to red (highest). The normalized contact distance d_{norm} is based on d_e, d_i and the van der Waals (vdW) radii of the two atoms external (r_e^{vdW}) and internal (r_i^{vdW}) to the surface:

$$d_{norm} = \frac{d_i - r^{vdW}}{r_i^{vdW}} + \frac{d_e - r}{r_e^{vdW}}$$

d_{norm} surface is used for the identification of very close intermolecular interactions. The value of d_{norm} is negative or positive when intermolecular r contacts are shorter or longer than r^{vdW}, respectively.

1.6 Calculations of Tanabe-Sugano (T-S) Matrices. The crystal field *D*q, Racah B parameters and tree correction α were obtained using the modified energy terms derived by Tanabe and Sugano as follows:

$^6S \rightarrow {}^4A_1; {}^4E({}^4G) = 10B + 5C + 20\alpha$

$^6S \rightarrow {}^4E({}^4D) = 17B + 5C + 6\alpha$

$^6S \rightarrow {}^4T_2({}^4D) = 13B + 5C + 8\alpha$

$^6S \rightarrow {}^4T_2({}^4G) = -10Dq + 18B + 6C - (26B^2/10Dq) + 22\alpha$

Calculated results: Dq = 910.06, B = 1647.6, C = 1169.8 and α = 25.3 for **1** and Dq = 673.4, B = 1194, C = 1847.8 and α = -80 for **2**.

2.Supporting figures

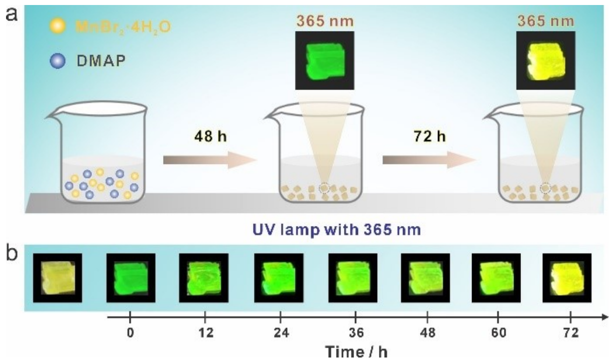

Fig. S1. (a) Synthesis process of two compounds by slow evaporation method. (b) Photographs of bulk crystals under natural light and 365 nm-UV lamp.

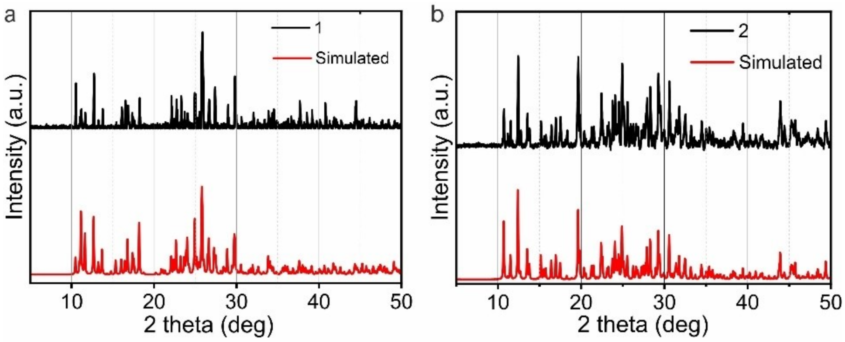

Fig. S2. Experimental and simulated powder XRD data of (a) **1** and (b) **2**.

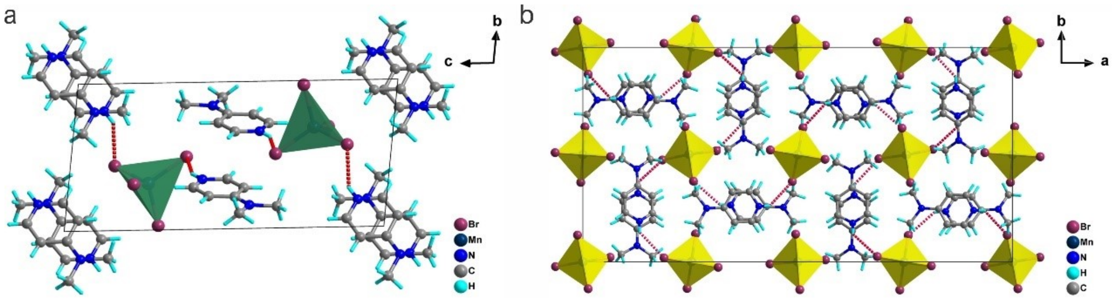

Fig. S3. 3D packing patterns of (a) **1** and (b) **2**, where isolated 0D $MnBr_4$ tetrahedral structures and protonated $DMAPH^+$ cations can be linked with each other by intermolecular N-H···Br bindings.

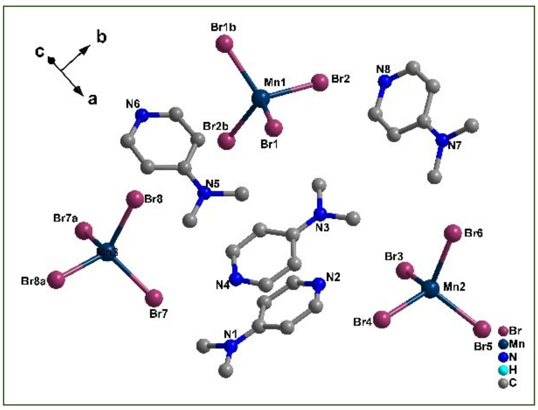

Fig. S4. Asymmetric unit of **2**.

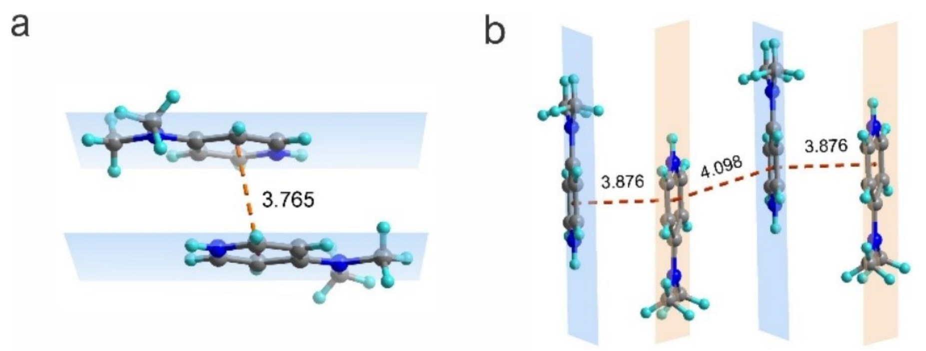

Fig. S5. π…π stacking interactions between organic cations in (a) **1** and (b) **2**.

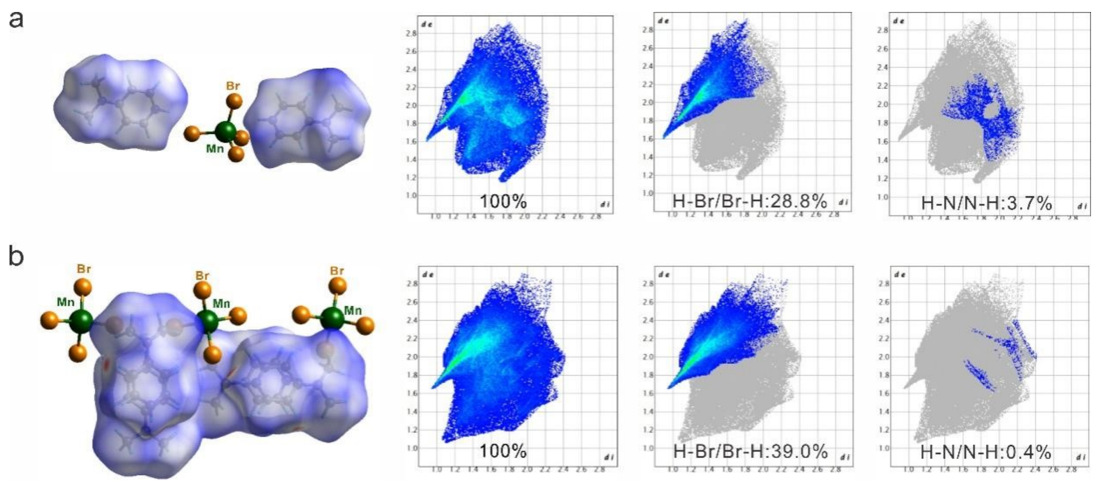

Fig. S6. Hirshfeld surfaceand 2D fingerprint of the DMPAH$^+$ cations in the asymmetric unit of (a) **1** and (b) **2**.

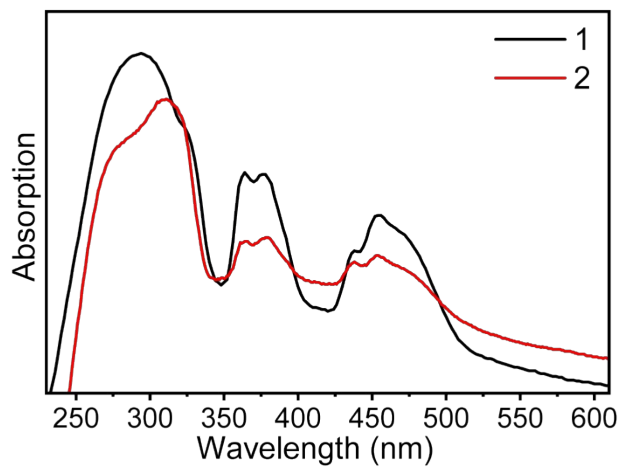

Fig. S7. UV-vis absorption spectra of **1** and **2**.

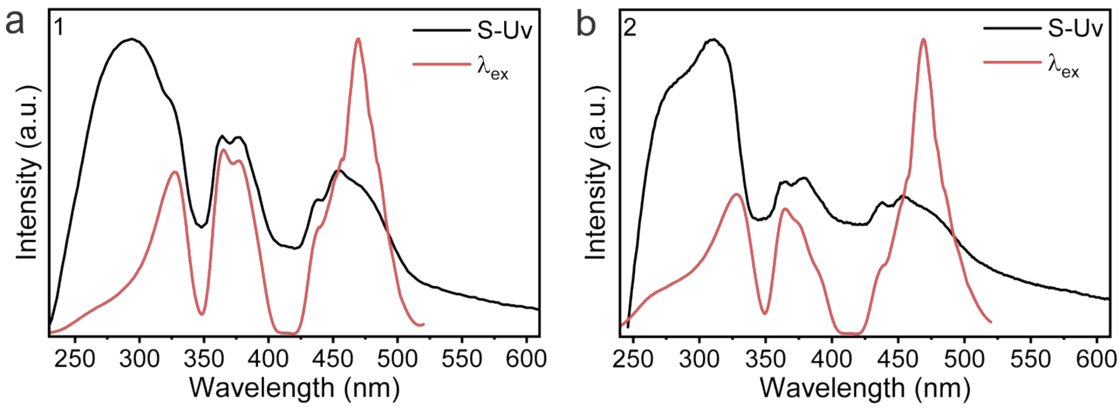

Fig. S8. UV-vis absorption and PLE spectra of (a) **1** and (b) **2**.

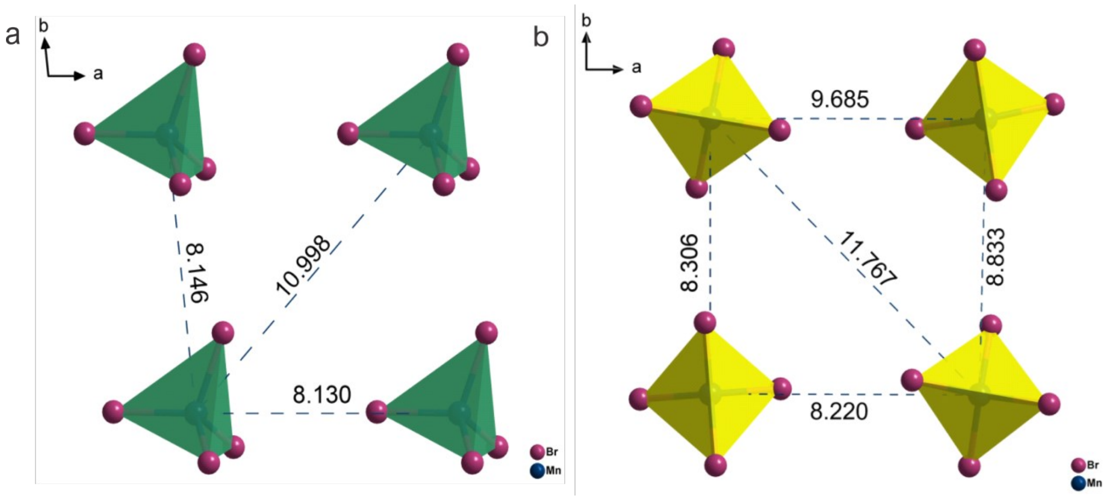

Fig. S9. Mn-Mn distance of (a) **1** and (b) **2**.

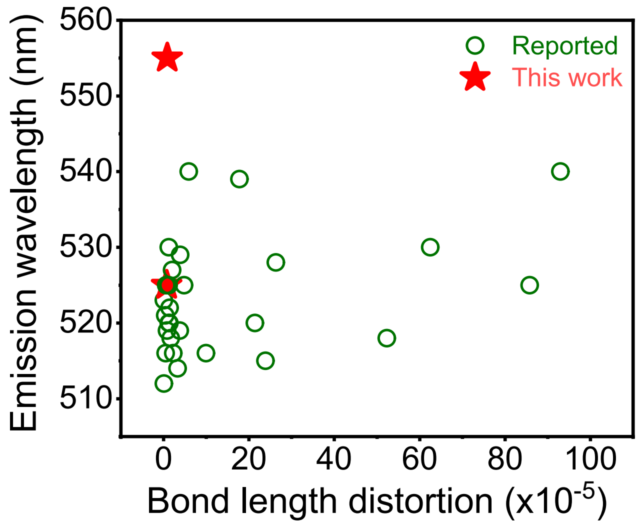

Fig. S10. Dependence of the emission wavelength on the bond length distortion in 0D tetrabromide hybrids.

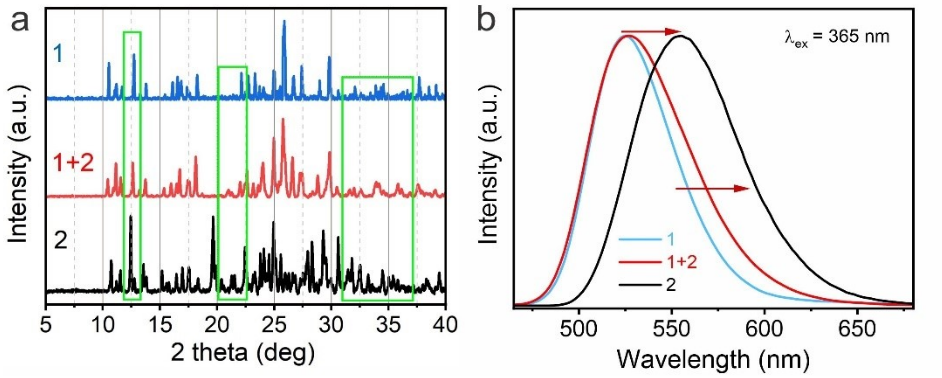

Fig. S11. (a) PXRD data and (b) PL spectra of **1**, **2**, and the sample with mixed phases.

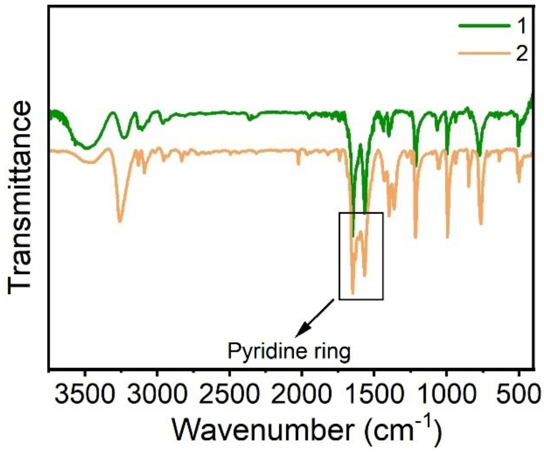

Fig. S12. FT-IR spectra of two compounds.

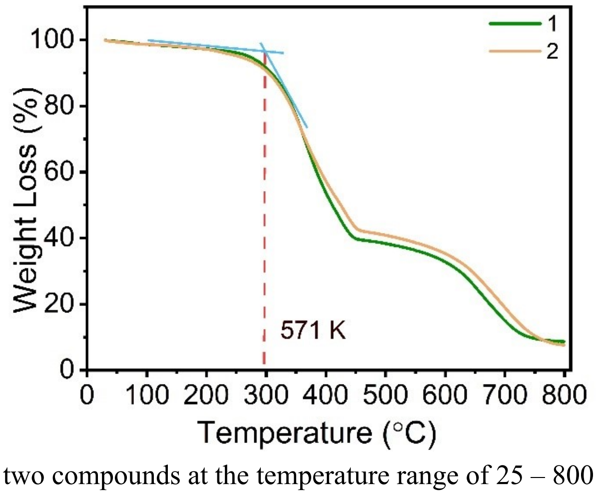

Fig. S13. TGA data of two compounds at the temperature range of 25 – 800 °C.

3. Supporting tables

Table S1. Crystal data of **1** and **2**.

Compound	**1**	Reported **1** [1]	**2**
Formula	$C_{14}H_{22}Br_4MnN_4$	$C_{14}H_{22}Br_4MnN_4$	$C_{14}H_{22}Br_4MnN_4$
Mr	620.93	620.90	1241.87
T/K	293(2)	111(2)	293(2)
Crystal system	Triclinic	Triclinic	Orthorhombic
Space group	P-1	P-1	$P2_12_12$
Z	2	2	4
a/Å	8.1305(3)	7.9747(4)	33.1106(6)
b/Å	8.1462(3)	8.0327(3)	16.5169(3)
c/Å	17.3017(6)	17.1042(5)	7.9113(2)
α/°	95.203(3)	101.556(3)	90
β/°	100.992(3)	94.407(3)	90
γ/°	94.982(3)	96.649(4)	90
V/Å^3	1113.97(7)	1060.59(7)	4326.57(16)
ρ_{calc}/gcm^{-3}	1.851	1.994	1.907
μ/mm^{-1}	7.770	8.160	8.001
F(000)	598.0	598.0	2392.0
Size/mm^3	0.1 × 0.1 × 0.05	-	0.1 × 0.1 × 0.1
S	1.021	-	1.041
R_{int}/R_{sigma}	0.0324/0.0444	0.0937	0.0480/0.0537
Reflections	20080	13049	10876
Data/Para.	5355/0/212	-	10876/0/424
R_1^a, wR_2^b [I>2σ(I)]	0.0527/0.1305	0.0441/0.0623	0.0441/0.0623
R_1^a, wR_2^b (all data)	0.0969/0.1528	-/0.1800	0.0966/0.0728
$\Delta\rho_{max}/\Delta\rho_{min}$ / e Å^{-3}	2.27/-0.97	2.65/-0.1.83	0.42/-0.60

$^aR_1 = \sum||F_o|-|F_c||/\sum|F_o|$. $^bwR_2 = [w(F_o^2-F_c^2)^2/w(F_o^2)^2]^{1/2}$

Table S2. Selective bond lengths and bond angles of **1**.

Atom-Atom	**Length/Å**	**Atom-Atom**	**Length/Å**
Mn1-Br1	2.5119(10)	Mn1-Br2	2.5098(11)
Mn1-Br3	2.4957(11)	Mn1-Br4	2.5116(11)
Atom-Atom-Atom	**Angle/°**	**Atom-Atom-Atom**	**Angle/°**
Br2-Mn1-Br4	105.27(4)	Br3-Mn1-Br4	111.72(4)
Br2-Mn1-Br1	111.18(4)	Br3-Mn1-Br1	108.89(4)
Br3-Mn1-Br2	109.20(4)	Br4-Mn1-Br1	110.56(4)

TableS3. Selective bond lengths and bond angles of **2**.

Atom-Atom	**Length/Å**	**Atom-Atom**	**Length/Å**
Mn2-Br3	2.5185(11)	Mn1-Br1	2.5001(10)
Mn2-Br6	2.5118(12)	Mn3-Br8	2.5036(10)
Mn1-Br2	2.5163(10)	Mn2-Br4	2.4935(12)
Mn2-Br5	2.5051(12)	Br7-Mn3	2.5008(10)
Atom-Atom-Atom	**Angle/°**	**Atom-Atom-Atom**	**Angle/°**
Br2-Mn1-Br2b	113.85(6)	Br4-Mn2-Br3	106.09(4)
Br1-Mn1-Br2	105.23(2)	Br4-Mn2-Br6	116.13(5)
Br1b-Mn1-Br2b	105.22(2)	Br4-Mn2-Br5	108.89(4)
Br1b-Mn1-Br2	107.74(2)	Br8a-Mn3-Br8	117.82(7)
Br1-Mn1-Br2b	107.74(2)	Br7-Mn3-Br8	105.58(2)
Br1b-Mn1-Br1	117.37(7)	Br7-Mn3-Br8a	105.38(2)
Br6-Mn2-Br3	105.69(4)	Br7a-Mn3-Br8a	105.58(2)
Br5-Mn2-Br3	114.62(5)	Br7a-Mn3-Br8	105.38(2)
Br5-Mn2-Br6	105.69(4)	Br7-Mn3-Br7a	117.76(7)

Symmetric code: (a) 1-*x*,1-*y*, +*z*; (b) 1-*x*,2-*y*, +*z*

Table S4. Bond length distortion and bond angle variance of $MnBr_4$ units, PL properties, and Huang-Rhys factor (*S*) for **1** and **2**.

Comp.	Units	Δd	σ^2	λ_{ex}	FWHM	τ / μs	S	PLQY
1	$MnBr_4^{2-}$	7.2×10^{-6}	5.44	525 nm	51 nm	198.48	1.12	80%
	$Mn^1Br_4^{2-}$	10.4×10^{-6}	24.72					
2	$Mn^2Br_4^{2-}$	1.4×10^{-5}	22.32	555 nm	68 nm	236.06	37.40	99.8%
	$Mn^3Br_4^{2-}$	3.1×10^{-7}	40.43					

Table S5. Bond length distortion and bond angle variance of previously reported $MnBr_4$ units.

Compound	Δd	σ^2	λ_{em} / nm
$(DMAPH)_2MnBr_4$ (**this work**)	8.1×10^{-6}	29.2	555
$([C_{16}Py]_2MnBr_4)$ [2]	9.3×10^{-4}	25.99	540
$(C_{13}H_{14}N)_2MnBr_4$ [3]	1.78×10^{-4}	24.64	539
$([C_{16}mim]_2MnBr_4)$ [2]	6.25×10^{-4}	23.38	530
$(3AMP)_2MnBr_4$ [4]	3.3×10^{-5}	21.51	514
$Mn(ttpo)Br_2$ [5]	0.097	19.41	512
$(KC)_2MnBr_4$ [6]	2.14×10^{-4}	14.72	520
$[MeIM]_2[MnBr_4]$ [7]	3.89×10^{-5}	12.87	529
$(3MP)_2MnBr_4$ [4]	9.1×10^{-7}	12.77	523
$(TMPEA)_2MnBr_4$ [4]	1.225×10^{-5}	12.59	520
$(HTPP)_2MnBr_4$ [8]	4.83×10-5	12.54	525
$[P_{14}]MnBr_4$ [9]	1.375×10^{-5}	10.75	520
$[PP_{14}]MnBr_4$ [9]	2.0×10^{-5}	10.74	527
$(Bz(Me)_3N)_2MnBr_4$ [10]	9.94×10^{-5}	10.53	516
$(HEP)_2MnBr_4$ [4]	8.02×10^{-6}	9.35	519
$(PrTPP)_2MnBr_4$ [11]	1.69×10^{-5}	9.3	518
PEA_2MnBr_4 [12]	1.24×10^{-5}	8.87	530
$[BTEA]_2MnBr_4$ [13]	3.88×10^{-6}	6.15	521
$(C_{13}H_{26}N)_2MnBr_4$ [3]	2.39×10^{-4}	6.08	515
$(BTMA)_2MnBr_4$ [14]	2.3×10^{-5}	5.8	516
$(DMAPH)_2MnBr_4$ (**this work**)	7.18×10^{-6}	5.44	525
$[EtIM]_2[MnBr_4]$ [7]	3.78×10^{-5}	5.29	519
$[(H_2CQCHCH_2)(C_6H_5)_3P]_2MnBr_4$ [15]	4.9×10^{-6}	4.9	516
$(MDPA)_2MnBr_4$ [16]	5.89×10^{-5}	4.32	540
$(C_{10}H_{16}N)_2MnBr_4$ [17]	5.23×10^{-4}	4.3	518
$[(CH_2)_4N(CH_2)_4]_2[MnBr_4]$ [18]	6.49×10^{-6}	4.3	525
$DIPA_2MnBr_4$ [10]	1.18×10^{-5}	2.66	525
$(BuTPP)_2MnBr_4$ [11]	1.4×10^{-5}	1.5	522
$(C_9H_{20}N)_2MnBr_4$ [19]	2.63×10^{-5}	/	528

Reference

[1] R. Babu, A. Samanta, S. Prasanthkumar, L. Polavarapu. Zn(II) Alloying Improves the Luminescence Efficiency of Hybrid Tetrahedral Mn(II) Halides ($(DMAPH)_2MnX_4$; X = Cl, Br, and I) to Near-Unity. *ACS Mater. Lett.*, **2023**, *5*, 2131-2138.

[2] S. Zhang, Y. Zhao, Y. Zhou, M. Li, W. Wang, H. Ming, X. Jing, S. Ye. Dipole-Orientation-Dependent Förster Resonance Energy Transfer from Aromatic Head Groups to $MnBr_4^{2-}$ Blocks in Organic–Inorganic Hybrids. *J. Phys. Chem. Lett.*, **2021**, *12*, 8692-8698.

[3] Q. Ren, J. Zhang, Y. Mao, M.S. Molokeev, G. Zhou, X.-M. Zhang. Ligand Engineering Triggered Efficiency Tunable Emission in Zero-Dimensional Manganese Hybrids for White Light-Emitting Diodes. *Nanomaterials*, **2022**, *12*, 3142.

[4] L. Mao, P. Guo, S. Wang, A.K. Cheetham, R. Seshadri. Design Principles for Enhancing Photoluminescence Quantum Yield in Hybrid Manganese Bromides. *J. Am. Chem. Soc.*, **2020**, *142*, 13582-13589.

[5] J. Lu, J. Gao, S. Wang, M.-J. Xie, B.-Y. Li, W.-F. Wang, J.-R. Mi, F.-K. Zheng, G.-C. Guo. Improving X-ray Scintillating Merits of Zero-Dimensional Organic–Manganese(II) Halide Hybrids via Enhancing the Ligand Polarizability for High-Resolution Imaging. *Nano Lett.*, **2023**, *23*, 4351-4358.

[6] J. Zhao, T. Zhang, X.-Y. Dong, M.-E. Sun, C. Zhang, X. Li, Y.S. Zhao, S.-Q. Zang. Circularly Polarized Luminescence from Achiral Single Crystals of Hybrid Manganese Halides. *J. Am. Chem. Soc.*, **2019**, *141*, 15755-15760.

[7] S. Shimono, M. Sekine, Y. Niwa, H. Sagayama, K. Araki, Y. Hata, H. Kishimura. Solid–liquid transitions in Mn-based ionic liquids $[MeIM]_2[MnBr_4]$ and $[EtIM]_2[MnBr_4]$ producing emission spectra with narrow green bands. *Mater. Res. Bull.*, **2023**, *159*, 112103.

[8] J.B. Luo, J.H. Wei, Z.Z. Zhang, Z.L. He, D.B. Kuang. A Melt-Quenched Luminescent Glass of an Organic–Inorganic Manganese Halide as a Large-Area Scintillator for Radiation Detection. *Angew. Chem. Int. Ed.*, **2023**, *62*, e202216504.

[9] L.-K. Gong, Q.-Q. Hu, F.-Q. Huang, Z.-Z. Zhang, N.-N. Shen, B. Hu, Y. Song, Z.-P. Wang, K.-Z. Du, X.-Y. Huang. Efficient modulation of photoluminescence by hydrogen bonding interactions between inorganic $[MnBr_4]^{2-}$ anions and organic cations. *Chem. Commun.*, **2019**, *55*, 7303-7306.

[10] V. Morad, I. Cherniukh, L. Pöttschacher, Y. Shynkarenko, S. Yakunin, M.V. Kovalenko. Manganese(II) in Tetrahedral Halide Environment: Factors Governing Bright Green Luminescence. *Chem. Mater.*, **2019**, *31*, 10161-10169.

[11] C. Sun, H. Lu, C.-Y. Yue, H. Fei, S. Wu, S. Wang, X.-W. Lei. Multiple Light Source-Excited Organic Manganese Halides for Water-Jet Rewritable Luminescent Paper and Anti-Counterfeiting. *ACS Appl. Mater. Interfaces*, **2022**, *14*, 56176-56184.

[12] W. Gao, M. Leng, Z. Hu, J. Li, D. Li, H. Liu, L. Gao, G. Niu, J. Tang. Reversible luminescent humidity chromism of organic–inorganic hybrid PEA2MnBr4 single crystals. *Dalton Trans.*, **2020**, *49*, 5662-5668.

[13] Y. Guo, J. Wu, W. Liu, S.-P. Guo. Organic Cation Modulation Triggered Second Harmonic Response in Manganese Halides with Bright Fluorescence. *Inorg. Chem.*, **2022**, *61*, 11514-11518.

[14] H. Fu, C. Jiang, J. Lao, C. Luo, H. Lin, H. Peng, C.-G. Duan. An organic–inorganic hybrid ferroelectric with strong luminescence and high Curie temperature. *CrystEngComm*, **2020**, *22*,

1436-1441.
[15] A. Jana, V.G. Sree, Q. Ba, S.C. Cho, S.U. Lee, S. Cho, Y. Jo, A. Meena, H. Kim, H. Im. Efficient organic manganese(ii) bromide green-light-emitting diodes enabled by manipulating the hole and electron transport layer. *J. Mater. Chem. C*, **2021**, *9*, 11314-11323.
[16] J. Lin, M. Zhang, N. Sun, S. He, X. Zhang, Z. Guo, J. Zhao, Q. Liu, W. Yuan. Narrowing the band of green emission in manganese hybrids by reducing the hydrogen bond strength and structural distortion. *J. Mater. Chem. C*, **2022**, *10*, 16773-16780.
[17] G. Zhou, Z. Liu, J. Huang, M.S. Molokeev, Z. Xiao, C. Ma, Z. Xia. Unraveling the Near-Unity Narrow-Band Green Emission in Zero-Dimensional Mn^{2+}-Based Metal Halides: A Case Study of (C10H16N)2Zn1–xMnxBr4 Solid Solutions. *J. Phys. Chem. Lett.*, **2020**, *11*, 5956-5962.
[18] L. Xu, J.-X. Gao, X.-G. Chen, X.-N. Hua, W.-Q. Liao. A temperature-triggered triplex bistable switch in a hybrid multifunctional material: $[(CH_2)_4N(CH_2)_4]_2[MnBr_4]$. *Dalton Trans.*, **2018**, *47*, 16995-17003.
[19] M. Li, J. Zhou, M.S. Molokeev, X. Jiang, Z. Lin, J. Zhao, Z. Xia. Lead-Free Hybrid Metal Halides with a Green-Emissive $[MnBr_4]$ Unit as a Selective Turn-On Fluorescent Sensor for Acetone. *Inorg. Chem.*, **2019**, *58*, 13464-13470.